Theoretical Analysis of the Excited States in Maleimide

Teresa Climent, Remedios González-Luque, and Manuela Merchán*

Departamento de Química Física, Instituto de Ciencia Molecular, Universitat de València, Dr. Moliner 50, Burjassot, ES-46100 Valencia, Spain

Received: December 9, 2002; In Final Form: May 20, 2003

The electronic excited states of maleimide have been studied using multiconfigurational second-order perturbation theory in its multistate formulation (MS-CASPT2) and extended atomic natural orbital (ANO) basis sets. The calculation of the singlet−singlet and singlet−triplet transition energies comprises 10 valence singlet excited states, four valence triplet states, and the singlet 3s, 3p, and 3d members of the Rydberg series converging to the first four ionization limits. The main features of the absorption spectrum correspond to the $1^1A_1 \rightarrow 1^1A_2(n\pi^*)$, $1^1A_1 \rightarrow 1^1B_2(\pi\pi^*)$, and $1^1A_1 \rightarrow 2^1B_2(\pi\pi^*)$ transitions computed at 3.29, 4.44, and 5.59 eV, respectively. The latter corresponds to the most intense band. The lowest Rydberg state is found to be at 5.98 eV in the high-energy side of the main band. A number of additional features are predicted in the higher-energy region of the spectrum, and our assignments follow the same trends as those offered earlier by Robin for *N*-methyl maleimide. The lowest triplet state is computed of $n\pi^*$ character in vacuo. However, arguments are given to rationalize the observed phosphorescence of maleimide in solution as being mainly of $\pi\pi^*$ nature.

1. Introduction

Cyclic imides are of fundamental importance in the realms of photochemistry and biochemistry, as well as commonly used reagents in organic and polymer chemistry. From a rapid literature review of the past few years, one can easily conclude that maleimides, apart from their classical function as photoinitiators,[1] are frequently used for a variety of purposes. Among them, a few selected applications are antitumor agents research,[2] study of membrane protein structure and function,[3] and development of new diagnostic devices and photochromic molecules.[4] It is also worth recalling the polyimides, polymers of recognized interest to the electronic industry because of their advantageous thermal and mechanical properties and low dielectric constant.[5] All of these applications rely on the well-known behavior of maleimides as efficient cross-linker units. Nature also exploits this ability to design chromoproteins. For instance, open-chain tetrapyrroles serve as chromophores in light sensor proteins of plants, phytochromes (P). The conversion of the physiological P-inactive form into the P-active form is photochromic and behaves as a light-driven biological switch.[6] Research on the photocycle of phytochromes is currently under way in our group accompanying recent work on choromophores related to rhodopsins[7] and photoactive yellow protein (PYP).[8] In the three cases, the key process involves a cis → trans and trans → cis double-bond photoisomerization. The view of maleimides as a building block of linear tetrapyrroles has actually been our main motivation to undertake the present study.

Despite the relevance of maleimides, to the best of our knowledge, there are no ab initio results published on the excited states of the simplest member of the family, maleimide (1*H*-pyrrole-2,5-dione). The electronic spectra of maleimides are, however, known since long ago.[9−13] In the energy region up to 6.5 eV, the recorded absorption spectrum can be described as composed of three bands in increasing order of intensity and transition energy. That the lowest-energy transition in the singlet manifold has $n\pi^*$ character with a very weak intensity was established in 1971 by Seliskar and McGlynn.[9] In the absorption spectrum of maleimide in EPA mixed solvent at 77 K, the feature at 3.33 eV was considered by these authors as the probable 0−0 band of this transition.[9] The second- and third-energy bands are assumed to involve excited states of $\pi\pi^*$ nature, which is confirmed in the present work. Among the available experimental data, we have chosen to compare to the maleimide data in solution using water as solvent (band maxima at 4.46 and 5.72 eV)[13] and the *N*-methyl maleimide vapor-phase data (transitions at 4.34 and 5.53 eV).[9,12] In the absorption spectrum of maleimide in water, the feature at 3.60 eV can be related to the $n\pi^*$ transition, which really looks like a shoulder of the second-energy band.[13] Ideally, our results for maleimide computed in vacuo should be compared with the corresponding observed spectrum in the vapor (not recorded so far). Therefore, we have to bear in mind two effects in the current comparison, as appropriate: solvent effects in a polar medium such as water or the methyl substitution or both. Nevertheless, taking into account the experimental information, the substitution effect could be regarded of minor importance. Thus, the theoretical findings will be preferably contrasted to the vapor data for *N*-methyl maleimide. It especially holds true for the Rydberg excited states because of their collapse in solution. A number of Rydberg transitions and additional valence excited states have been identified in the vapor (*N*-methyl maleimide).[9,12] Information about the triplet states comes from the phosphorescence spectra of maleimides in EPA solvent at 77 K.[9] It was concluded that the $T_1 \rightarrow S_0$ transition in maleimide and its N-alkyl derivatives involves a triplet state of $n\pi^*$ nature. As shall be discussed below, the situation is more complex, and it is likely that the observed phosphorescence in solution comes mainly from a triplet state of $\pi\pi^*$ character, although the lowest two triplet states computed in vacuo are both of $n\pi^*$ type.

During the past decade, we have devoted considerable effort to characterize theoretically the excited states of a large number of fundamental organic compounds.[14−16] Maleimide is a basic

10.1021/jp0225572 CCC: $25.00
Published on Web 08/19/2003

heterocyclic polyene of intrinsic importance.[12] Previous works performed on related molecules such as pyrrole[17] and imidazole[18] give insight on the complexity of the problem. In addition, the theoretical spectroscopy of the carbonyl group addressed in different studies (formaldehyde,[19] acetone,[20] *p*-benzoquinone[21]) points out the inherent difficulties implied in a dione. We report here a comprehensive theoretical research study of the excited states of maleimide, both of valence and Rydberg nature. We shall find that the previous descriptions are largely vindicated, but the situation is shown to be even more complicated than previously suspected. The excited states of the system have been characterized by using multiconfigurational second-order perturbation theory through the CASPT2 method.[22,23] In addition, the indirect interaction of the resulting states has been taken into account within the framework of the multistate CASPT2 (MS-CASPT2) method.[24] The successful performance of the CASPT2 approach to the interpretation of the electronic spectra of a large number of organic compounds is well established.[14−16] The study performed on maleimide includes determination of vertical excitation energies, band origin, and emission maximum for the electronic transitions involving the low-lying valence excited states of the singlet and triplet manifold. We believe that the present results give a more complete picture for a better understanding, on theoretical grounds, of the spectroscopic behavior of maleimides and provide confident assignments. They serve both to complement earlier studies and to bring a firm theoretical foundation to elucidate the photochemistry of maleimide.

The paper is organized as follows. Computational details are described in the next section. After that, the equilibrium geometry of the ground and low-lying excited states are considered. Results and analysis on the computed singlet → singlet and singlet → triplet absorption spectra and 0−0 transition are subsequently considered, together with comparison to previous findings. Our conclusions are summarized in the last section.

2. Theoretical Methods and Computational Details

Generally contracted basis sets of atomic natural orbitals type (ANO) obtained from the C,N,O(14s9p4d)/H(8s4p) primitive sets with the C,N,O[4s3p1d]/H[2s1p] contraction scheme[25] were used for the geometry optimization of the ground and low-lying valence excited states at the CASSCF level. For the geometry determination of the ground and low-lying excited states of $\pi\pi^*$ nature, the active space comprised the eight π-valence electrons distributed among the seven π-valence molecular orbitals (MOs). The active space was enlarged with the corresponding lone pair MO, CASSCF(8 MOs/10 electrons), for the description of the respective $n\pi^*$ states.

In the computation of the excitation energies, the basis set was supplemented with a 1s1p1d set of Rydberg functions (contracted from a set of 8s8p8d primitives). They were built following the protocol described elsewhere.[14] Because of the relatively close spacing of the highest four occupied MOs (see Figure 1), the 3s-, 3p-, and 3d-Rydberg members converging to the lowest four ionization potentials are expected to overlap. In addition, the valence excited states would be interleaved among the Rydberg states. The low-lying Rydberg states of interest are described mainly by a one-electron promotion from the natural orbitals of the type $3b_1(\pi_1)$, $2b_1(\pi_2)$, $9b_2(lp_1)$, and $12a_1(lp_2)$ to the corresponding Rydberg orbital. Accordingly, the 1s1p1d Rydberg functions were placed at the averaged charge centroid of the 1^2B_1, 2^2B_1, 1^2B_2, and 1^2A_1 states of the maleimide cation determined at the π-CASSCF level (plus lone pair lp_1 or lp_2). The final basis set consists of a total of 150 functions (559 primitives). The spectroscopic results reported here were computed including Rydberg functions.

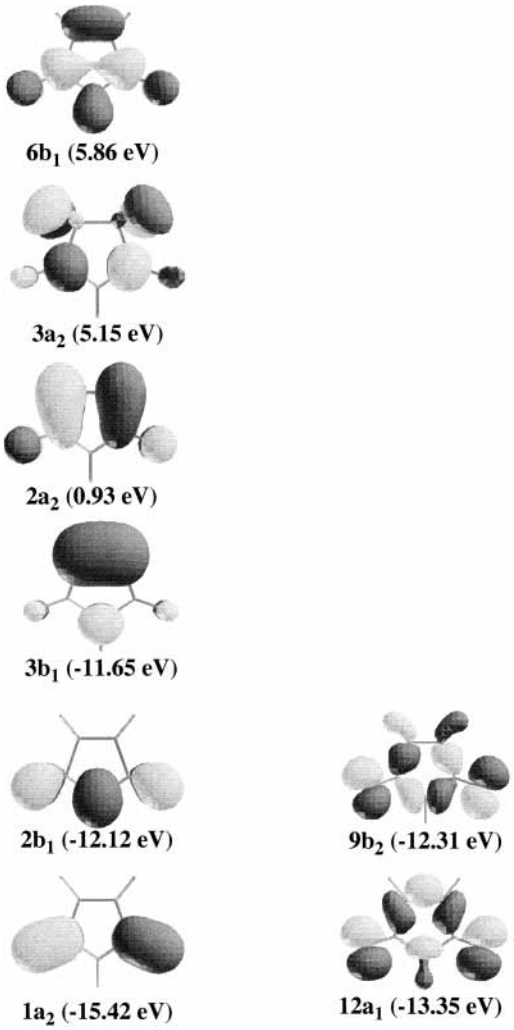

Figure 1. Highest five occupied and lowest three unoccupied canonical MOs and SCF orbital energies computed with the ANO-type C,N,O-[4s3p1d]/H[2s1p] basis set at the ground-state π-CASSCF equilibrium geometry.

Multiconfigurational wave functions were initially determined at the CASSCF level.[26] For the vertical excitation energies, the carbon, nitrogen, and oxygen 1s electrons were kept frozen in the form determined by the ground-state closed-shell Hartree−Fock wave function. The total SCF energy for the ground state (1^1A_1) of maleimide was calculated to be −357.534 785 au. The eight π electrons were always chosen to be active. The π-valence active space is denoted by (0;4;0;3), where the entries indicate the number of active orbitals belonging to the irreducible representations a_1, b_1, b_2, and a_2, respectively, of the point group C_{2v}. The active space was extended to include the Rydberg orbitals of symmetry $a_1(3s, 3p_z, 3d_{z^2}, 3d_{x^2-y^2})$, $b_1(3p_x, 3d_{xz})$, $b_2(3p_y, 3d_{yz})$, and $a_2(3d_{xy})$, as appropriate. The active spaces used and the states computed are listed in Table 1.

Later, the relative vertical energy of each excited stated is referenced to the ground-state energy computed with the same active space. The MOs for the excited states were obtained from average CASSCF computations, where the averaging includes all states of interest within a given symmetry. The number of states included in the state average CASSCF calculations is compiled in Table 1, together with the number of configurations involved in the CASSCF wave function.

TABLE 1: CASSCF Wave Functions Employed To Compute the Excited States of Maleimide with the ANO-type Basis Set C,N,O[4s3p1d]/H[2s1p] + 1s1p1d Rydberg Functions

wave function[a]	$(N_e)^b$	states	$N_{configurations}{}^c$	$N_{states}{}^d$
		Singlet Excited States Involving lp_1 (Inactive: 8;0;5;0)		
CASSCF (4;4;1;3)	(10)	$^1B_2(lp_1\rightarrow 3s, 3p_z, 3d_{z^2}, 3d_{x^2-y^2})$	42336	7
CASSCF (0;6;1;3)	(10)	$^1A_2(lp_1\rightarrow\pi^*,3p_x,3d_{xz})$; $^1A_2(lp_1\pi\rightarrow\pi^*\pi^*)$	4424	4
CASSCF (0;4;3;3)	(10)	$^1A_1(lp_1\rightarrow 3p_y,3d_{yz})$	4984	6
CASSCF (0;4;1;4)	(10)	$^1B_1(lp_1\rightarrow\pi^*,3d_{xy})$	1176	2
		Singlet Excited States Involving lp_2 (Inactive: 7;0;6;0)		
CASSCF (5;4;0;3)	(10)	$^1A_1(lp_2\rightarrow 3s,3p_z,3d_{z^2},3d_{x^2-y^2})$	43030	7
CASSCF (1;6;0;3)	(10)	$^1B_1(lp_2\rightarrow\pi^*,3p_x,3d_{xz})$	4424	3
CASSCF (1;4;2;3)	(10)	$^1B_2(lp_2\rightarrow 3p_y,3d_{yz})$	4840	5
CASSCF (1;4;0;4)	(10)	$^1A_2(lp_2\rightarrow\pi^*,3d_{xy})$	1176	2
		Singlet Excited States of $\pi\pi^*$ Nature (Inactive: 8;0;6;0)		
CASSCF (4;4;0;3)	(8)	$^1B_1(\pi_1\rightarrow 3s,3p_z,3d_{z^2},3d_{x^2-y^2})$		
		$^1B_1(\pi_2\rightarrow 3s,3p_z,3d_{z^2},3d_{x^2-y^2})$	8176	8
CASSCF (0;6;0;3)	(8)	$^1A_1(\pi\pi^*)$;$^1A_1(\pi_1\rightarrow 3p_x,3d_{xz})$		
		$^1A_1(\pi\pi^*)$;$^1A_1(\pi_2\rightarrow 3p_x,3d_{xz})$	2688	7
CASSCF (0;4;2;3)	(8)	$^1A_2(\pi_1\rightarrow 3p_y,3d_{yz})$; $^1A_2(\pi_2\rightarrow 3p_y,3d_{yz})$	1280	4
CASSCF (0;4;0;4)	(8)	$^1B_2(\pi\pi^*)$; $^1B_2(\pi\pi^*)$; $^1B_2(\pi\pi^*)$		
		$^1B_2(\pi_1\rightarrow 3d_{xy};\pi_2\rightarrow 3d_{xy})$	864	5

[a] Within parentheses are the number of orbitals of the symmetries a_1, b_1, b_2, and a_2, respectively, of the point group C_{2v}. Number of frozen orbitals = (4;0;3;0). Number of occupied SCF MOs = (12;3;9;1). [b] Number of active electrons. [c] Number of configurations in the CASSCF wave function. [d] States included in the average CASSCF wave function.

To take into account the remaining correlation effects, the CASSCF wave functions were employed as reference functions in a single-state second-order perturbation CASPT2 treatment.[22,23] In addition, the effect of weakly interacting intruder states was minimized by using the so-called imaginary level-shift technique.[27] After careful calibration calculations, the shift of 0.2 au was selected to compile the final results. Even in cases where it was really not needed, the computation has been carried out at the same level shift because the energy results are not altered (at most 0.05 eV) and it renders consistency to the different comparisons performed (excitation energies, ionization potentials, singlet−triplet splitting, and so on). The coupling of the CASSCF wave functions via dynamic correlation was dealt with by using the extended multistate CASPT2 approach, the MS-CASPT2 method.[24] An effective Hamiltonian matrix is constructed where the diagonal elements correspond to the CASPT2 energies and the off-diagonal elements introduce the coupling to second order in the dynamic correlation energy. In this way, all states of a given symmetry can be treated simultaneously with the correlation effects on the reference functions included, and the possible erratic valence−Rydberg mixing can be removed yielding an effective separation of the computed states, which can be clearly identified as valence and Rydberg excited states. For a case of strong valence−Rydberg mixing and its successful solution at the MS-CASPT2 level, the reader is referred to the recent study on the anti conformer of *n*-tetrasilane.[28]

The CASSCF state interaction (CASSI) method[29,30] was used to calculate the transition dipole moments from the perturbation modified CAS (PMCAS) reference functions (the model states),[24] i.e., linear combinations of all CAS states involved in the MS-CASPT2 calculation. In the formula for the oscillator strength, the PMCAS-CI transition moment and the energy difference obtained in the MS-CASPT2 computation were used.

All calculations were performed with the MOLCAS-5 quantum-chemistry software.[31]

3. Results and Discussion

As a preliminary step toward the theoretical understanding of the electronic spectrum of maleimide, the geometry of the ground state and low-lying singlet and triplet excited states are first considered. The properties of the excited states computed vertically are next analyzed. After that, the nonvertical transition energies are discussed. Furthermore, the present findings will be compared with the available experimental data and previous theoretical descriptions obtained at the semiempirical level.

3.1. Equilibrium Structures. Geometry optimizations for the ground state and low-lying excited states of both $\pi\pi^*$ and $n\pi^*$ character were carried out at the π-CASSCF level ($\pi\pi^*$) and at the same level enlarging the active space with the lone pair of the oxygen atoms ($n\pi^*$). The optimized geometric parameters for the ground state and singlet and triplet excited states are depicted in Figure 2. Optimizations were constrained to C_{2v} symmetry with the molecule placed in the *yz* plane, *z* being the C_2 axis passing along the N−H bond.

The bond lengths computed for the ground state are similar to the gas-phase molecular structure determined by electron diffraction (ED)[32] (r(C═C) = 1.344 Å, r(C−C) = 1.508 Å, r(N−C) = 1.409 Å, r(C═O) = 1.206 Å), consistent with a C_{2v} symmetry model. In the ED study, the N−H and C−H bond lengths were assumed to be 1.025 and 1.096 Å, respectively. Both are somewhat too long compared to the π-CASSCF results and other theoretical determinations.[32,33] Therefore, the fact that the larger deviation between the computed geometric parameters and the experimental data occurs in the N−C bond distance (1.383 vs 1.409 Å) could be related to the assumptions made in the ED research with a N−H distance fixed at a too long value. Similar comments are appropriate to rationalize the deviation on the computed CCH angle of 122.3° (cf. Figure 2) with respect to the experimentally derived datum (114.7°).[32] Even when the known sensitivity of the carbonyl bond distance upon the level of theory is taken into consideration,[19,20] the π-CASSCF trends are consistent with previous structure determination of ground-state maleimide performed at the ab initio and semiempirical levels.[32] Therefore, it might be worth redoing the ED analysis employing the theoretical results instead of the above-mentioned assumed values.

From the nature of the canonical MOs determined of the ground state (see Figure 1), four low-lying singlet and triplet excited states can be predicted, as actual computation confirms. The minus and plus linear combinations of the in-plane lone-pair of the oxygen atoms lead to the $9b_2(lp_1)$ and $12a_1(lp_2)$ MOs. The one-electron promotion from lp_1 to the lowest unoccupied

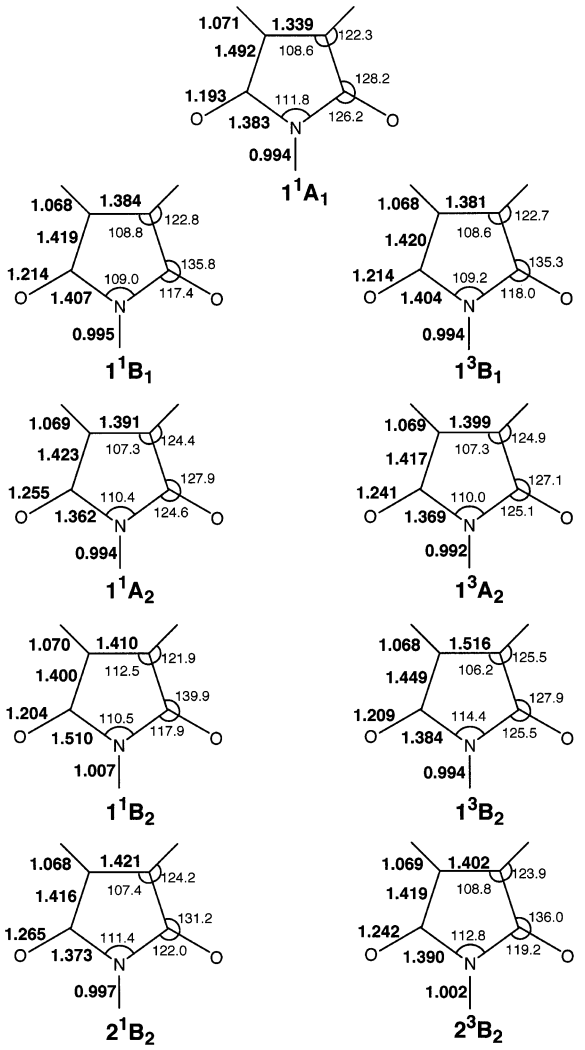

Figure 2. Geometries optimized at the π-CASSCF level (1^1A_1, $1^{1,3}B_2$, and $2^{1,3}B_2$ states) and with the active space enlarged with the lone pairs MOs of the oxygen atoms ($1^{1,3}B_1$ and $1^{1,3}A_2$) as appropriate. Bond lengths given in Å and angles in deg.

molecular orbital (LUMO), $2a_2$, gives rise to the 1^1B_1 and 1^3B_1 states with the two electrons singlet- or triplet-coupled, respectively. Similarly, the $1^1A_2(lp_2 \rightarrow \pi^*)$ and $1^3A_2(lp_2 \rightarrow \pi^*)$ states can also be expected, where π^* represents a LUMO-like molecular orbital. There are also two singlet and two triplet states of B_2 symmetry as plausible candidates to appear in the low-energy region. They involve charge transfer from the highest occupied molecular orbital (HOMO) and HOMO − 1 into LUMO. Because there is electron reorganization within the π system in these states with respect to the ground state, they shall be labeled $\pi\pi^*$. The orbital energies between the HOMO ($3b_1$) and the HOMO − 1 ($2b_1$) differ in only 0.47 eV. Therefore, it is not surprising that they can be mixed in the CASSCF procedure, in accordance with the variational principle, to yield natural orbitals rotated with respect to the canonical MOs. Indeed, analysis of the homologous CASSCF natural orbitals (denoted by prime hereafter) reveals that they are mainly localized in the nitrogen atom ($2b_1'$) and the other in the C=C region ($3b_1'$). In terms of the natural orbitals, the two lowest $\pi\pi^*$ states are described by the corresponding singly excited configurations from a b_1'-type to the LUMO-like natural orbital. In all the cases, the LUMO-like natural orbital maintains its topology as the canonical LUMO ($2a_2$) shown in Figure 1. Analysis of the obtained excited-state geometric trends in terms

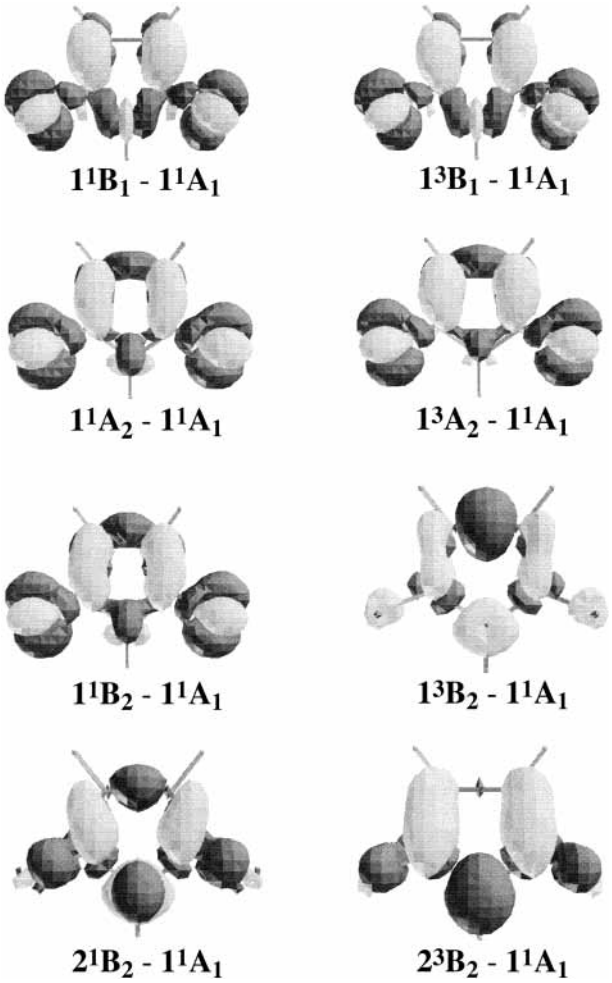

Figure 3. Density difference with respect to the ground state for the eight electronic excited states in their respective equilibrium geometry.

of the configurations involved is, therefore, a laborious task because of the different sets of natural orbitals that have to be detailed simultaneously. We have preferred to rationalize the computed molecular structures in terms of the electron density difference (EDD) between the ground and the excited state at the equilibrium geometry of the excited state. Thus, to analyze in more detail the relationship between the electronic nature and equilibrium geometry, the computed EDDs for the eight low-lying excited states of valence character are shown in Figure 3.

The darkest surfaces (plotted at an electronic density of 0.004 electrons/au^3) represent regions where the density difference is negative—"where the electron comes from". By a rapid inspection of Figure 3, one can easily notice the involvement and the important role of the LUMO-like orbital in the description of the eight excited states. Accordingly, the increase of electron density in the two C−C regions of the excited state is paralleled by a decrease of the two equivalent C−C bond distances. To a lesser or greater extent, it holds true for all of the cases considered. For the $n\pi^*$ transitions the electron density is moved from the lone-pair MOs (lp_1 or lp_2), causing an elongation of the carbonyl bond length. A pronounced increase of the N−C and C=C bond distances occurs for the $1^1B_2(\pi\pi^*)$ and 1^3B_2-$(\pi\pi^*)$ states, respectively, in accordance with the electron density shift from those respective regions. Conversely, by inspection of the EDDs related to the $2^1B_2(\pi\pi^*)$ and $2^3B_2(\pi\pi^*)$ electronic states, one can understand the lengthening of the C=O bond distance taking place in these excited states.

TABLE 2: Computed PMCAS-CI and MS-CASPT2 Excitation Energies (eV), Related Oscillator Strengths (*f*), and PMCAS-CI Dipole Moments (μ, D) for the Vertical Excited States of Maleimide, Employing the C,N,O[4s3p1d]/H[2s1p] + 1s1p1d (Rydberg Functions) ANO-type Basis Set and Available Experimental Data

state[a]	PMCAS-CI	MS-CASPT2	*f*	μ	exptl
ground state (1^1A_1)				−1.78	
		Singlet Excited States			
$1^1B_1(lp_1\rightarrow\pi^*)$	6.99	2.48	0.0004	−0.16	
$1^1A_2(lp_2\rightarrow\pi^*)$	7.97	3.29	*b*	−0.08	3.33(0−0),[c] 3.60[d]
$1^1B_2(\pi\pi^*)$	6.61	4.44	0.0221	+0.50	4.34,[e] 4.46[d]
$2^1B_2(\pi\pi^*)$	8.67	5.59	0.4526	−0.92	5.53,[e] 5.72[d]
$3^1B_2(lp_1\rightarrow 3s)$	9.86	5.98	0.0318	−3.23	
$2^1A_2(lp_1\rightarrow\pi^*)$	11.46	6.00	*b*	−1.80	
$3^1A_2(lp_1\pi\rightarrow\pi^*\pi^*)$	11.17	6.35	*b*	−0.40	
$4^1A_2(lp_1\rightarrow 3p_x)$	10.40	6.75	*b*	−1.94	
$4^1B_2(lp_1\rightarrow 3p_z)$	10.36	6.78	0.0000	+0.89	
$2^1A_1(lp_1\rightarrow 3p_y)$	9.47	6.84	0.0356	+1.83	
$3^1A_1(lp_2\rightarrow 3s)$	9.49	6.96	0.0727	−3.54	6.99,[e] 6.94[f]
$4^1A_1(\pi\pi^*)$	8.31	7.13	0.0335	+1.18	6.99,[e] 6.94[f]
$2^1B_1(lp_2\rightarrow\pi^*)$	12.36	7.30	0.0000	−0.84	
$3^1B_1(\pi_1\rightarrow 3s)$	7.56	7.35	0.0001	−3.90	
$5^1A_2(lp_1\rightarrow 3d_{xz})$	10.98	7.38	*b*	+2.40	
$5^1B_2(lp_1\rightarrow 3d_{z^2})$	10.86	7.41	0.0001	+3.33	
$4^1B_1(lp_1\rightarrow 3d_{xy})$	10.44	7.62	0.0003	+0.41	
$5^1A_1(lp_2\rightarrow 3p_z)$	10.20	7.67	0.0134	+2.01	7.81[f]
$5^1B_1(lp_2\rightarrow 3p_x)$	10.99	7.75	0.0005	−1.40	
$6^1B_2(lp_1\rightarrow 3d_{x^2-y^2})$	11.15	7.77	0.0083	+0.94	
$7^1B_2(lp_2\rightarrow 3p_y)$	11.92	7.79	0.0005	+1.79	
$6^1A_1(lp_1\rightarrow 3d_{yz})$	10.11	7.80	0.0016	−1.26	
$6^1B_1(\pi_2\rightarrow 3s)$	8.41	7.81	0.0259	+1.84	
$7^1B_1(\pi_1\rightarrow 3p_z)$	8.41	8.20	0.0014	+2.88	
$7^1A_1(\pi_1\rightarrow 3p_x)$	7.62	8.22	0.0099	−1.06	
$8^1A_1(lp_2\rightarrow 3d_{z^2})$	10.71	8.28	0.0218	+2.61	
$8^1B_2(lp_2\rightarrow 3d_{yz})$	12.39	8.42	0.0045	−2.49	
$6^1A_2(lp_2\rightarrow 3d_{xy})$	11.47	8.50	*b*	+0.38	
$9^1A_1(\pi\pi^*)$	9.72	8.53	0.0160	+1.04	8.13,[e] 8.12[f]
$7^1A_2(\pi_1\rightarrow 3p_y)$	8.32	8.54	*b*	+3.94	
$8^1B_1(\pi_2\rightarrow 3p_z)$	9.03	8.56	0.0022	−1.24	
$9^1B_1(lp_2\rightarrow 3d_{xz})$	11.66	8.61	0.0011	+2.01	
$10^1A_1(lp_2\rightarrow 3d_{x^2-y^2})$	10.89	8.66	0.0077	+1.03	8.68[f]
$11^1A_1(\pi_2\rightarrow 3p_x)$	8.54	8.74	0.0272	−0.51	
$10^1B_1(\pi_1\rightarrow 3d_{z^2})$	8.93	8.77	0.0029	+5.85	
$9^1B_2(\pi\pi^*)$	10.42	8.77	0.0151	−0.23	
$8^1A_2(\pi_2\rightarrow 3p_y)$	9.03	8.93	*b*	+3.04	
$12^1A_1(\pi_1\rightarrow 3d_{xz})$	8.44	9.00	0.0001	+4.68	
$10^1B_2(\pi_1\rightarrow 3d_{xy})$	9.37	9.00	0.0292	+1.98	
$9^1A_2(\pi_1\rightarrow 3d_{yz})$	8.81	9.14	*b*	+0.71	
$11^1B_1(\pi_1\rightarrow 3d_{x^2-y^2})$	9.20	9.23	0.0008	+2.14	
$12^1B_1(\pi_2\rightarrow 3d_{z^2})$	9.73	9.26	0.0101	−8.69	
$11^1B_2(\pi_2\rightarrow 3d_{xy})$	10.14	9.42	0.0000	−3.28	
$13^1A_1(\pi_2\rightarrow 3d_{xz})$	9.32	9.62	0.0000	−6.69	
$10^1A_2(\pi_2\rightarrow 3d_{yz})$	9.81	9.69	*b*	−11.66	
$13^1B_1(\pi_2\rightarrow 3d_{x^2-y^2})$	10.08	9.73	0.0054	−2.67	
		Triplet Excited States			
$1^3B_1(lp_1\rightarrow\pi^*)$	6.34	2.31		+0.08	
$1^3A_2(lp_2\rightarrow\pi^*)$	7.34	3.14		+0.15	
$1^3B_2(\pi\pi^*)$	4.12	3.49		−2.52	
$2^3B_2(\pi\pi^*)$	5.21	3.84		+1.16	

[a] The character and ordering of the states are those obtained with the MS-CASPT2 method. [b] Forbidden. [c] From the absorption spectrum of maleimide in EPA mixed solvent at 77 K.[9] [d] From the absorption spectrum of maleimide in water.[13] [e] From the vapor absorption spectrum of *N*-methyl maleimide.[9] [f] From the vapor absorption spectrum of *N*-methyl maleimide.[12]

The optimized geometries were employed to characterize the vertical electronic spectrum (absorption and emission) and nonvertical electronic transitions. These topics will be treated in turn.

3.2. Vertical Spectra of Maleimide. The computed vertical excitation energies at the PMCAS-CI and MS-CASPT2 levels of theory, together with oscillator strengths of the corresponding transitions, dipole moments, and selected experimental data are listed in Table 2. The nature of the states, valence or Rydberg, as computed from the corresponding PMCAS-CI wave function, has been characterized on the basis of the dominant orbital configurations and the expectation values $\langle x^2\rangle$, $\langle y^2\rangle$, and $\langle z^2\rangle$, which are appreciably larger for Rydberg states than are those of the ground state and valence excited states. The resulting assignment of the excited state is given within parentheses in the first column of Table 2, identifying the different excited states of maleimide. The detailed interpretation of the results is discussed below.

Valence Singlet Excited States. At the highest level of theory employed, four valence singlet excited states are placed below the lowest Rydberg transition. They correspond to the excited states presented in the previous section and can be related to

the main features of the recorded electronic spectrum up to 6 eV. The two lowest singlet excited states are of $n\pi^*$ type, the $1^1B_1(lp_1 \rightarrow \pi^*)$ and $1^1A_2(lp_2 \rightarrow \pi^*)$ states, and are calculated to lie vertically 2.48 and 3.29 eV above the ground state, respectively. The intensities of the transitions are predicted to be exceedingly weak. In fact, the $1^1A_1 \rightarrow 1^1A_2$ electronic transition is electric-dipole-forbidden. The computed excitation energy for the 1^1A_2 state is consistent with the spectroscopic data of maleimide in EPA with a band origin at 3.33 eV.[9] The band maximum moves up to 3.60 eV in the maleimide absorption spectrum in water.[13] From the magnitude of the dipole moment of the valence excited states with respect to that of the ground state, the occurrence of a blue shift in polar solvents can be predicted qualitatively for most of the valence transitions considered. Therefore, considering the uncertainty in the experimental determination of the band-origin peak, the error bars of the computation (0.1−0.2 eV), and the solvent influence, the agreement between theory and experiment can be regarded at first sight as satisfactory. Nevertheless, the situation is actually more complex. Vibronic interactions with the higher-energy allowed $\pi\pi^*$ state, through the activity of out-of-plane vibrations, are proposed as the source of the observed intensity in the lowest-energy band of maleimide, similarly as it is documented to occur for the forbidden $n\pi^*$ transition in the simplest carbonyl compound, formaldehyde,[19] and homologous (also forbidden) transitions in related systems such as *p*-benzoquinone.[21] It is worth recalling that in the observed spectrum of maleimide,[13] the $n\pi^*$ feature looks like a shoulder of the lowest-energy $\pi\pi^*$ band. The energy difference of the computed band origin for the $1^1A_1 \rightarrow 1^1A_2$ transition and the vertical excitation is 0.59 eV (see below). It is consistent with the expected long Franck−Condon progression because of the pronounced geometric changes taking place in the excited state with respect to the ground state (see Figure 2). In the recorded spectrum, the band maximum could easily be somewhat deviated from the band origin and the vertical transition. Moreover, the overall contribution of the lowest excited state (1^1B_1) to the observed feature is difficult to predict at present, although it is expected to play a minor role. Therefore, in case that a higher accuracy would be required to fully describe on theoretical grounds the observed low-intensity, low-energy band of maleimide, vibronic interactions would have to be taken into account and the two lowest excited states would have to be considered. The $n\pi^*$ transitions have been previously obtained at the semiempirical level, but the lowest excited state, 1^1B_1, instead of the second excited state, 1^1A_2, was assigned to be responsible for the observed band in view of the forbidden character of the electronic transition involving the latter.[9]

There has been controversy along the years concerning the character, valence or Rydberg, of the main bands of maleimide. From the MS-CASPT2 results, it is clear that both the second- and third-energy observed bands can be related each to a single electronic transition: $1^1A_1 \rightarrow 1^1B_2$ and $1^1A_1 \rightarrow 2^1B_2$, respectively. Both are valence $\pi\pi^*$ transitions, the former with the vertical transition computed at 4.44 eV and the latter at 5.59 eV. Comparatively, the lowest $\pi\pi^*$ transition is weaker than the third-energy band, predicted to be the most intense feature of the absorption spectrum of maleimide in the gas phase. Nevertheless, the lowest Rydberg excited state is predicted in the higher-energy side of the third-energy band. The theoretical findings are consistent with the high-pressure effect investigation reported by Robin.[12] Both transitions show vibrational structure in the vapor absorption spectrum on *N*-methyl maleimide with band maximum at 4.34 and 5.53 eV.[9] In solution, only the third-energy band of maleimide is structured. The respective band maxima are slightly blue-shifted to 4.46 and 5.72 eV.[13] Despite the large Stokes shifts predicted from the optimized geometries of the excited states involved, the relative concordance of the recorded band maximum with the corresponding excitation energy computed vertically seems to point out that the description of the lowest $\pi\pi^*$ electronic transitions within the Franck−Condon scheme is appropriate.

TABLE 3: Computed CASSCF and CASPT2 Vertical Ionization Potentials (IP) Employing the C,N,O[4s3p1d]/H[2s1p] + 1s1p1d (Rydberg functions) ANO-type Basis Set[a]

IP	state	CASSCF	CASPT2
IP_1	$1^2B_2(lp_1\text{-hole})$	11.33	9.41
IP_2	$1^2A_1(lp_2\text{-hole})$	12.35	10.32
IP_3	$1^2B_1(\pi_1\text{-hole})$	9.95	10.61
IP_4	$2^2B_1(\pi_2\text{-hole})$	11.19	11.08
IP_5	$1^2A_2(\pi\text{-hole})$	12.75	13.43
IP_6	$3^2B_1(\pi\text{-hole})$	15.37	15.30

[a] The character and ordering of the states are those obtained with the CASPT2 method. Results in eV.

Higher valence excited states are predicted at 6.00, 6.35, 7.13, 7.30, 8.53, and 8.77 eV (MS-CASPT2 results). They are related to the excited states $2^1A_2(lp_1 \rightarrow \pi^*)$, $3^1A_2(lp_1\pi \rightarrow \pi^*\pi^*)$, $4^1A_1(\pi\pi^*)$, $2^1B_1(lp_2 \rightarrow \pi^*)$, $9^1A_1(\pi\pi^*)$, and $9^1B_2(\pi\pi^*)$, respectively. The 2^1A_2 state involves a one-electron promotion from the lp_1 MO to the valence orbital $3a_2$. The 3^1A_2 state is of mixed character, implying simultaneous electron promotion from the lp_1 and occupied π orbitals. The related transitions are electric-dipole-forbidden and are expected to play a minor role in the description of the spectrum. Transition from the ground to the 2^1B_1 state, described mainly by the singly excited configuration $lp_2 \rightarrow \pi^*$ (b_1-type), is also predicted with a weak intensity. The remaining valence excited states, 4^1A_1, 9^1A_1, and 9^1B_2, are of $\pi\pi^*$ character. Those two of the same symmetry as the ground state show complex multiconfigurational wave functions. The 4^1A_1 state has a large weight (31%) of the configuration involving the two-electron promotion $(HOMO \rightarrow LUMO)^2$. It is the expected doubly excited state. The placement of a valence transition at about 7 eV, overlapped with a transition $n \rightarrow 3s$ (cf. Table 2), is consistent with previous suggestion.[12] A feature observed at 8.12 eV of vertical nature was deduced by Robin to be of valence $\pi\pi^*$ character in the gas spectrum of *N*-methyl maleimide.[12] It can be tentatively related here to the $1^1A_1 \rightarrow 9^1A_1$ transition computed at 8.53 eV, although the $1^1A_1 \rightarrow 8^1A_1$ Rydberg transition at 8.28 eV has a larger oscillator strength and is energetically closer to the detected peak. The 9^1B_2 state is the highest valence state computed (8.77 eV) and can be described primarily by the one-electron promotion from the $2b_1'$ MO to the valence MO $3a_2$ (weight 75%).

Rydberg Singlet Excited States. The calculations comprise the 3s, 3p, and 3d members of the Rydberg series converging to the first four ionization potentials (IPs). Table 3 lists the vertical IPs computed at the CASSCF and CASPT2 levels. A comparison of the CASSCF and CASPT2 results demonstrates the importance of dynamic correlation effects for an accurate prediction of the IPs, which are highly differential for the different states of the maleimide cation. Indeed, the lowest IP at the CASSCF level is computed to have a π-hole in the cation whereas the actual ground state of the maleimide cation is the $1^2B_2(lp_1\text{-hole})$ state. The energy difference between the CASPT2 and the CASSCF results gives the effect of dynamic correlation on the obtained IPs, clearly larger for the *n*-hole states than for π-hole states. It points out the difficulties that approximate methods may encounter in the treatment of maleimide, a very

complex molecule to be described on theoretical grounds, although at first sight it may appear to be simple because of its relatively small molecular size.

The first (IP_1) and second (IP_2) vertical ionization potentials of maleimide lie within 0.9 eV of each other (CASPT2 results). As a consequence, corresponding members of the Rydberg series converging to these two ionization potentials are expected to lie within 1 eV of each other. Consistently, the energy difference between the $3^1A_1(lp_2 \rightarrow 3s)$ and $3^1B_2(lp_1 \rightarrow 3s)$ is 0.98 eV at the MS-CASPT2 level. The $3^1B_1(\pi_1 \rightarrow 3s)$ state appears at 7.35 eV, 0.39 eV above the $3^1A_1(lp_2 \rightarrow 3s)$ state. The energy difference can be related to the difference $IP_3 - IP_2$ (0.29 eV). The placement of the $6^1B_1(\pi_2 \rightarrow 3s)$ state at 7.81 eV, 0.46 eV above the $3^1B_1(\pi_1 \rightarrow 3s)$ state, also keeps the trend ($IP_4 - IP_3 = 0.47$ eV). Because 1.5 eV approximates the usual 3s and 3d Rydberg-state separation, Rydberg states leading to the first four ionized limits are expected to overlap in energy even for the early series members. Here we discuss the MS-CASPT2 energies and assignments for the states described by excitations out of the lp_1-, lp_2-, π_1-, and π_2-like MOs and compare them with the experimental assignments performed in *N*-methyl maleimide in the gas phase.[12]

The calculated vertical transition energy from the ground to the lowest 3s Rydberg state, $3^1B_2(lp_1 \rightarrow 3s)$, is 5.98 eV. The oscillator strength is around 0.03. It is predicted at the high-energy region of the most intense band. In the gas-phase absorption spectrum of maleimide, the 3s Rydberg feature would probably look like a sharp peak overlapping the vibrational structure of the strongest $\pi\pi^*$ band. This prediction is consistent with the findings reported by Robin concerning the optical spectrum of *N*-methyl maleimide vapor. Robin investigated the high-pressure effect on the 5.53-eV band and found that the 0−0 and a few higher vibronic bands remained sharp under perturbation but several others displayed the broadening to higher frequencies characteristic of Rydberg transitions. Consequently, it was suggested that certain members of the $\pi\pi^*$ vibronic band are strongly mixed with the $n \rightarrow 3s$ Rydberg excitation.[12] The assignment from the current results is clear: the Rydberg state involved in the mixing is precisely the $3^1B_2(lp_1 \rightarrow 3s)$ state.

The $4^1A_2(lp_1 \rightarrow 3p_x)$ state is calculated to lie 6.75 eV above the ground state. Transitions to the $4^1B_2(lp_1 \rightarrow 3p_z)$ and $2^1A_1(lp_1 \rightarrow 3p_y)$ states appear slightly above, at 6.78 and 6.84 eV, respectively. The former is predicted to be exceedingly weak, and the latter has a computed oscillator strength similar to that obtained for the $1^1A_1 \rightarrow 3^1B_2(lp_1 \rightarrow 3s)$ transition.

The energy of the first component of the Rydberg series to the second ionization potential is computed to be 6.96 eV. The $1^1A_1 \rightarrow 3^1A_1(lp_2 \rightarrow 3s)$ transition has a significant oscillator strength, 0.07. It is observed at 6.94−6.99 eV in *N*-methyl maleimide.[9,12] In the same energy region, an overlapping valence shell transition (to the 4^1A_1 state) is predicted, in agreement with the conclusions achieved from the analysis performed by Robin.[12]

The members of the $lp_1 \rightarrow 3d$ series have been computed in the energy range 7.38−7.80 eV. The transitions are predicted with weak intensity. Within the same energy interval, the $1^1A_1 \rightarrow 5^1A_1(lp_2 \rightarrow 3p_z)$ transition at 7.67 eV is clearly allowed and can be related to the 3p assignment in *N*-methyl maleimide at 7.81 eV.[12] In addition, on the basis of expected term values, the peak at 8.68 eV in the methylated compound was assigned as a transition to 3d. This is consistent with the computed results for maleimide (cf. Table 2), in particular with the $1^1A_1 \rightarrow 10^1A_1(lp_2 \rightarrow 3d_{x^2-y^2})$ electronic transition computed at 8.66 eV. Because the symmetries of the transition moments are not known experimentally and many closely spaced states are calculated in the higher spectral region, coincidence between experimental and computed transition energy may be accidental. In this region, therefore, the experimental (*N*-methyl maleimide) and theoretical results (maleimide) can be best combined to deduce the spectral assignments (*N*-methyl maleimide), but neither can be said to confirm the other. We just realize that the assignments performed by Robin in *N*-methyl maleimide and our results on maleimide follow the same pattern. Larger deviation in the correlation between experimental data and theoretical results is obtained for the valence transition to the 9^1A_1 state. It is unclear whether the discrepancy is because of the influence of the methyl group, uncertainties in the experimental−theoretical correlation, limitations in the resolution of the observed spectrum, or limitations in our own calculations. However, both molecules have a similar scheme: a valence feature in maleimide (*N*-methyl maleimide) 8.53 (8.12 eV) is between two Rydberg peaks located at 7.67 (7.81) and 8.66 (8.68) eV.

Many closely spaced states are predicted in the energy region 9−9.7 eV. The average of the excitation energies corresponding to $\pi_1 \rightarrow 3d$ and $\pi_2 \rightarrow 3d$ is 9.03 and 9.54 eV, respectively. Thus, they are about half of an electronvolt apart from each other, as is the separation between the fourth and third ionization potentials computed vertically (0.47 eV).

Low-Lying Triplet Excited States. The singlet−triplet spectrum computed at the ground-state geometry places the lowest triplet state $1^3B_1(lp_1 \rightarrow \pi^*)$ at 2.31 eV. The second triplet state is also of $n\pi^*$ character and lies 3.14 eV above the ground state. The ordering and nature of the four lowest valence singlet and triplet states is similar. The $\pi\pi^*$ triplet states, 1^3B_2 and 2^3B_2, are found at 3.49 and 3.84 eV, respectively. Therefore, a considerably larger singlet−triplet splitting is computed for the $\pi\pi^*$ states than for the $n\pi^*$ states. It can be easily rationalized in terms of the exchange integral involved in the energy difference between a triplet and singlet state, both described by the same orbitals, in a simple molecular orbital model. Because the penetration of a $\sigma-\pi$ excitation is smaller than that of a $\pi-\pi^*$, the exchange integral is larger in the latter and consequently the singlet−triplet splitting is more pronounced.

One of the key questions of spectroscopy of maleimide is the source of the observed luminescence, mainly phosphorescence. A more detailed discussion on this topic shall be considered in the next section, involving the nonvertical features of the spectrum. We just mention here that from the dipole moments of the triplet states a slight blue shift for the $n\pi^*$ states and a red shift for the lowest $\pi\pi^*$ state can be inferred to occur in polar solvents.

3.3. Emission and Nonvertical Transition Energies of Maleimide. With the optimized geometry of the excited states, the corresponding emission and nonvertical features have also been characterized. Knowledge of the energy hypersurfaces of the ground and low-lying excited states of maleimides is essential for the determination of spectroscopic properties, which are particularly relevant in an ample group of biologically active chromophores. The basic understanding of the spectroscopic behavior of these compounds requires not only the accurate computation of the vertical states but also the characterization of the emission and nonvertical transition energies.

The computed transitions involve the energy difference between the ground and the excited state at the respective optimized geometry and the vertical emission from the excited-state minimum vertically to the ground state. The 0−0 absorption, also labeled T_0, is the first component of each absorption

TABLE 4: Vertical, Adiabatic, and Emission Electronic Transitions Computed for Maleimide[a]

	vertical absorption		0−0 transition		emission maximum	
state	PMCAS-CI	MS-CASPT2	PMCAS-CI	MS-CASPT2	PMCAS-CI	MS-CASPT2
			Singlet−Singlet Spectra			
$1^1B_1(lp_1 \rightarrow \pi^*)$	6.99	2.48	6.29	2.38	5.73	1.94
$1^1A_2(lp_2 \rightarrow \pi^*)$	7.97	3.29	7.20	2.70	6.71	2.43
$1^1B_2(\pi\pi^*)$	6.61	4.44	5.03	3.65	3.72	2.62
$2^1B_2(\pi\pi^*)$	8.67	5.59	7.78	4.99	7.05	4.55
			Singlet−Triplet Spectra			
$1^3B_1(lp_1 \rightarrow \pi^*)$	6.34	2.31	5.98	2.08	5.48	1.68
$1^3A_2(lp_2 \rightarrow \pi^*)$	7.34	3.14	6.91	2.48	6.47	2.21
$1^3B_2(\pi\pi^*)$	4.12	3.49	3.33	2.77	2.61	2.20
$^3B_2(\pi\pi^*)$	5.21	3.84	4.57	3.07	3.92	2.65

[a] Geometry has been optimized at the CASSCF level (see Figure 2). The ANO-type C,N,O[4s3p1d]/H[2s1p] enlarged with 1s1p1d diffuse functions has been used in the spectral study. Results in eV.

band and corresponds to a transition from and to the lowest vibrational state. The computed value is, however, T_e. The energy difference between T_0 and T_e is expected to be small in maleimide (within 0.1 eV). On the other hand, the vertical emission (fluorescence or phosphorescence) is obtained from experiment as the maximum of the emission band. The basis set includes diffuse functions, and the active spaces are those used in the geometry optimization and for the vertical transitions (π-valence plus lone pair MOs as appropriate). Then a consistent comparison can be performed between the computed absorption and emission spectra. The study includes determination of the adiabatic transition and emission maximum for the four lowest valence excited states in the singlet and triplet manifold. Because the geometry of the excited states has been optimized within the C_{2v} symmetry, the computed band origins can be considered upper bounds of the actual gas-phase data. On the other hand, considering that any deviation from planarity would certainly increase the energy of the ground state, the emission maxima might be somewhat smaller than those reported here. Table 4 lists the vertical, adiabatic, and fluorescence and phosphorescence maximum for the $n\pi^*$ and $\pi\pi^*$ states. The vertical ordering of the states is maintained in the adiabatic and emission transitions. For the lowest singlet−singlet feature ($n\pi^*$-type), the vertical and adiabatic transitions are computed within 0.1 eV, and the fluorescence maximum is predicted at 1.94 eV. The $1^1A_1 \rightarrow 1^1A_2$ with the band origin around 0.59 eV below the vertical feature seems to be responsible for the weak band overlapping the lowest $\pi\pi^*$ band. The computed origin at 2.70 eV can be compared to the datum reported for maleimide in EPA mixed solvent at 77 K, 3.33 eV.[9] As stated earlier, this is a complex band and its intensity should arise by vibronic coupling. Nevertheless, the deviation of the theoretical results with respect to the experimental is somewhat large, even invoking a blue shift due to solvent effects. In this respect, one should recall that the component located at 3.33 eV was considered as the most likely to be the 0−0 band, probably because it is the lowest feature recorded. It is clear that higher resolution in this energy region is required to determine accurately the band origin (and also the most intense peak, if different).

In the vapor absorption spectrum of *N*-methyl maleimide at 360 K, the 0−0 vibrational band of the lowest $\pi\pi^*$ band could not be determined because the onset of this transition was found to be weak, overlapping the $n\pi^*$ transition. However, by inspection of the observed spectrum (see Figure 3 in Seliskar and McGlynn[9]), the band origin is estimated to be around 3.5 eV, consistent with the computed result at 3.65 eV. We have related the third-energy band to the $1^1A_1 \rightarrow 2^1B_2$ electronic transition. The origin is computed at 4.99 eV, that is, 0.6 eV below the vertical transition. The absorption spectrum of *N*-methyl maleimide at 300 K (Figure 4 in Seliskar and McGlynn[9]), which is slightly unresolved because of instrumental limitations, has the most prominent peak at 5.53 eV. On the basis of the corresponding vibrational analysis, it was assigned by these authors as the band origin.[9] The prominent feature was subsequently classified as adiabatic−vertical by Robin.[12] The fact is that the recorded spectrum begins at 5.4 eV,[9] and the MS-CASPT2 result suggests that the origin should be around half an electronvolt below. Can the influence of the methyl group produce such a deviation? It is at present an open question. Once more, it is clear that a higher resolution of the vapor absorption spectrum of maleimides would be highly appreciated. It is also worth noting that the theoretical results, both vertical and adiabatic, are very reasonable compared to the absorption spectrum of maleimide in water,[13] where the full spectrum from 3.1 to 6.8 eV is depicted. A shift of 0.1−0.2 eV is easily rationalized because of solvent effects, including possible maleimide−water hydrogen bonding, and limitations of the computation.

Maleimide exhibits appreciable luminescence in solution, and its N-alkyl derivatives are only very weakly emissive. The emission appears to be solely of phosphorescent nature. The triplet excited state has been tentatively assigned to $n\pi^*$ character on the basis of the observed lifetime (10 ms) of the phosphorescence of maleimide in EPA mixed solvent at 77 K. Not much further evidence was given to support the assignment.[9] Because of the weak luminescence, it was difficult to locate accurately the 0−0 vibrational band. It was assumed to be at 2.80 eV, the first clear feature of the recorded phosphorescence spectrum, where a maximum around 2.50 eV can be also noted (see Figure 7 reported by Seliskar and McGlynn[9]).

The current results give an additional rationalization of the observed phosphorescence spectrum. The $1^1A_2(lp_2 \rightarrow \pi^*)$ and $1^3B_2(\pi\pi^*)$ states are computed to be, within the error bars of the method, nearly degenerate with adiabatic transitions at 2.70 and 2.77 eV. In fact, at the optimized geometry of the 1^1A_2 state, the 1^3B_2 state is found at 2.72 eV. The small energy gap between the two states and their different nature, $^1(n\pi^*)$ and $^3(\pi\pi^*)$, suggest that an efficient intersystem crossing can actually take place. The observed phosphorescence with an origin estimated at 2.80 eV and an emission maximum at 2.50 eV approximately is consistent with the computed results for the $1^3B_2 \rightarrow 1^1A_1$ transition, 2.77 eV (0−0) and 2.20 eV (emission maximum). The picture is further complicated by the occurrence of the emission maximum from the $1^3A_2(lp_2 \rightarrow \pi^*)$ state, which is also predicted at 2.21 eV. Thus, taking into account spin−orbit interactions, those states can further interact. It points out that phosphorescence comes mainly from the

$^3(\pi\pi^*)$ state with some mixing of $^3(n\pi^*)$ as suggested earlier by Scharf and Leismann.[11] Comparison of the dipole moment of the lowest triplet of $\pi\pi^*$ character and the ground state reveals that the excited state should suffer a larger stabilization in polar solvents; as a consequence, a red shift of the computed transition in vacuo can be expected. Using similar arguments, we can infer a slight blue shift for the triplet $n\pi^*$ transitions. Therefore, even if in the gas phase the lowest two triplet states are computed to be of $n\pi^*$ character, we suggest that the main source of the observed phosphorescence in solution comes most probably from a $\pi\pi^*$ triplet state.

4. Summary and Conclusions

The excited states of maleimide have been studied using ab initio quantum-chemical methods based on multiconfigurational wave functions. Forty-six singlet and four triplet excited states have been characterized. Employing the optimized geometry of the ground state at the CASSCF level, the vertical excitation energies have been computed with the MS-CASPT2 method. The calculation comprised both valence and Rydberg excited states in the singlet manifold. In particular, the 3s, 3p, and 3d members of the Rydberg series converging to the first four ionization potentials have been explicitly taken into account. Four valence singlet excited states have been identified below the lowest 3s Rydberg state. They have been related to the observed absorption spectrum of maleimide in solution and *N*-methyl maleimide in the gas phase. To estimate the band origin and emission maximum, geometry optimizations for the lowest four singlet and triplet excited states have also been performed at the CASSCF level.

We conclude that each of the three observed bands in the absorption spectrum of maleimide (up to 6 eV) is related to a single electronic excitation. The lowest-energy band has $n\pi^*$ character. The lone pair MO can be described as the symmetric linear combination of the lone pair of the oxygen atoms (a_1 symmetry in the C_{2v} point group), and the π^* is the LUMO. Transition to the 1^1A_2 state is therefore electric-dipole-forbidden, and the source of weak feature observed can be attributed to vibronic coupling. Below the 1^1A_2 state, the 1^1B_1 state is computed to be the lowest excited state. It is also of $n\pi^*$ character, where *n* represents the minus linear combination of the oxygen lone pairs (b_2 symmetry) and π^* is the LUMO. It seems that it has not been detected experimentally. The 1^1B_1 and 1^1A_2 states have been placed vertically at 2.48 and 3.29 eV, respectively. The second- and third-energy bands are of $\pi\pi^*$ nature. They have been related to the $1^1A_1 \rightarrow 1^1B_2$ (4.44 eV) and $1^1A_1 \rightarrow 2^1B_2$ (5.59 eV) electronic transitions, the latter predicted to be the most intense of the spectrum. The lowest Rydberg state is computed in the high-energy side of the most intense feature at 5.98 eV. The Rydberg states follow the trends expected from the computed ionization potentials and are interleaved among four dipole-allowed excited states of valence character placed vertically at 7.13, 7.30, 8.53, and 8.77 eV. The results complement the available data on the higher-energy region of the spectrum of *N*-methyl maleimide and show the same trends as those analyzed by Robin.

An attempt to rationalize the observed phosphorescence of maleimide has also been performed. In summary, we propose that the relaxation of the singlet state responsible for the lowest-energy band, the $1^1A_2(lp_2 \rightarrow \pi^*)$ state, causes the intersection between the $1^1A_2(lp_2 \rightarrow \pi^*)$ and $1^3B_2(\pi\pi^*)$ potential hypersurfaces in polar solvents, that is, an optimal situation for an efficient intersystem crossing. Therefore, the observed phosphorescence comes mainly from the triplet $1^3B_2(\pi\pi^*)$ state, which is predicted to be the lowest triplet state in solution. The results are consistent with the recorded phosphorescence pattern of maleimide in EPA.

Acknowledgment. Financial support from the MCYT of Spain through the Project BQU2001-2926 and by the Generalitat Valenciana is gratefully acknowledged.

References and Notes

(1) Miller, C. W.; Jönsson, E. S.; Hoyle, C. E.; Viswanathan, K.; Valente, E. J. *J. Phys. Chem. B* **2001**, *105*, 2707.
(2) Antczak, C.; Baubois, B.; Monneret, C.; Florent, J. C. *Bioorg. Med. Chem.* **2001**, *9*, 2843.
(3) Schopfer, L. M.; Salhany, J. M. *Anal. Biochem.* **1998**, *257*, 139.
(4) Liu, X. H.; Wang, H. K.; Herron, J. N.; Prestwich, G. D. *Bioconjugate Chem.* **2000**, *11*, 755.
(5) LaFemina, J. P.; Arjavalingam, G.; Hougham G. *J. Chem. Phys.* **1989**, *90*, 5154.
(6) Schaffner, K.; Gärtner, W. *The Spectrum* **1999**, *12*, 1.
(7) González-Luque, R.; Garavelli, M.; Bernardi, F.; Merchán, M.; Robb, M. A.; Olivucci, M. *Proc. Natl. Acad. Sci. U.S.A.* **2000**, *97*, 9379.
(8) Molina, V.; Merchán, M. *Proc. Natl. Acad. Sci. U.S.A.* **2001**, *98*, 4299.
(9) Seliskar, C. J.; McGlynn, S. P. *J. Chem. Phys.* **1971**, *55*, 4337.
(10) Seliskar, C. J.; McGlynn, S. P. *J. Chem. Phys.* **1972**, *56*, 1417.
(11) Scharf, H.-D.; Leismann, H. *Z. Naturforsch.* **1973**, *28*, 662.
(12) Robin, M. B. *Higher Excited States of Polyatomic Molecules*; Academic Press: New York, 1975; Vol. II.
(13) Johnson, E. A. In *UV−Vis Atlas of Organic Compounds*; Perkampus, H.-H., Ed.; VCH: Weinheim, Germany, 1992; p 175.
(14) Roos, B. O.; Fülscher, M. P.; Malmqvist, P.-Å.; Merchán, M.; Serrano-Andrés, L. In *Theoretical Studies of Electronic Spectra of Organic Molecules*; Langhoff, S. R., Ed.; Kluwer Academic Publishers: Dordrecht, The Netherlands, 1995; p 357.
(15) Roos, B. O.; Andersson, K.; Fülscher, M. P.; Malmqvist, P.-Å.; Serrano-Andrés, L.; Pierloot, K.; Merchán, M. In *Multiconfigurational Perturbation Theory: Applications in Electronic Spectroscopy*; Prigogine, I., Rice, S. A., Eds.; J. Wiley & Sons: New York, 1996; p 219.
(16) Merchán, M.; Serrano-Andrés, L.; Fülscher, M. P.; Roos, B. O. In *Multiconfigurational Perturbation Theory Applied to Excited States of Organic Compounds*; Hirao, K., Ed.; World Scientific Publishing Company: Amsterdam, 1999; Vol. 4, p 161.
(17) (a) Serrano-Andrés, L.; Merchán, M.; Nebot-Gil, I.; Roos, B. O.; Fülscher, M. *J. Am. Chem. Soc.* **1993**, *115*, 6184. (b) Roos, B. O.; Malmqvist, P.-Å.; Molina, V.; Serrano-Andrés, L.; Merchán, M. *J. Chem. Phys.* **2002**, *116*, 7526.
(18) Serrano-Andrés, L.; Fülscher, M. P.; Roos, B. O.; Merchán, M. *J. Chem. Phys.* **1996**, *100*, 6484.
(19) Merchán, M.; Roos, B. O. *Theor. Chim. Acta* **1995**, *92*, 227.
(20) Merchán, M.; Roos, B. O.; McDiarmid, R.; Xing, X. *J. Chem. Phys.* **1996**, *104*, 1791.
(21) (a) Pou-Amérigo, R.; Merchán, M.; Ortí, E. *J. Chem. Phys.* **1999**, *110*, 9536. (b) Pou-Amérigo, R.; Serrano-Andrés, L.; Merchán, M.; Ortí, E.; Forsberg, N. *J. Am. Chem. Soc.* **2000**, *122*, 6067.
(22) Andersson, K.; Malmqvist, P.-Å.; Roos, B. O.; Sadlej, A. J.; Wolinski, K. *J. Phys. Chem.* **1990**, *94*, 5483.
(23) Andersson, K.; Malmqvist, P.-Å.; Roos, B. O. *J. Chem. Phys.* **1992**, *96*, 1218.
(24) Finley, J.; Malmqvist, P.-Å.; Roos, B. O.; Serrano-Andrés, L. *Chem. Phys. Lett.* **1998**, *288*, 299.
(25) Widmark, P.-O.; Malmqvist, P.-Å.; Roos, B. O. *Theor. Chim. Acta* **1990**, 77, 291.
(26) For reviews of the CASSCF methods, see different contributions in: *Ab Initio Methods in Quantum Chem.-II*; Lawley, K. P., Ed.; J. Wiley & Sons Ltd.: New York, 1987.
(27) Forsberg, N.; Malmqvist, P.-Å. *Chem. Phys. Lett.* **1997**, *274*, 196.
(28) Crespo, R.; Merchán, M.; Michl, J. *J. Phys. Chem. A* **2000**, *104*, 8593.
(29) Malmqvist, P.-Å. *Int. J. Quantum Chem.* **1986**, *30*, 479.
(30) Malmqvist, P.-Å.; Roos, B. O. *Chem. Phys. Lett.* **1989**, *155*, 189.
(31) Andersson, K.; Baryz, M.; Bernhardsson, A.; Blomberg, M. R. A.; Boussard, P.; Cooper, D. L.; Fleig, T.; Fülscher, M. P.; Hess, B.; Karlström, G.; Lindh, R.; Malmqvist, P.-Å.; Neogrády, P.; Olsen, J.; Roos, B. O.; Sadlej, A. J.; Schimmelpfennig, B.; Schütz, M.; Seijo, L.; Serrano-Andrés, L.; Siegbahn, P. E. M.; Stålring, J.; Thorsteinsson, T.; Veryazov, V.; Wahlgren, U.; Widmark, P.-O. *MOLCAS*, version 5.0; Department of Theoretical Chemistry, Chemical Centre, University of Lund: Lund, Sweden, 2000.
(32) Harsányi, L.; Vajda, E.; Hargittai, I. *J. Mol. Struct.* **1985**, *129*, 315.
(33) Császár, P.; Császár, A.; Harsányi, L. *J. Mol. Struct.* **1986**, *136*, 323.